



Physicochemical characterization and molecular modeling study of host–guest systems of aripiprazole and functionalized cyclodextrins

Ionuț-Mihai Tănase¹ · Laura Sbârcea² · Adriana Ledetiș³ · Gabriela Vlase⁴ · Paul Barvinschi⁵ · Renata-Maria Văruț⁶ · Anca Dragomirescu⁷ · Carmen Axente³ · Ionuț Ledetiș^{1,8}

Received: 7 October 2019 / Accepted: 13 March 2020 / Published online: 21 March 2020
© Akadémiai Kiadó, Budapest, Hungary 2020

Abstract

Aripiprazole (ARP), an innovative atypical antipsychotic drug, exhibits very low aqueous solubility, affecting its dissolution and absorption and high lipophilicity. Its complexation with cyclodextrins (CDs) was designed to improve drug solubility and consequently its bioavailability. The inclusion complexes of aripiprazole with two β -cyclodextrin derivative, namely random methyl- β -cyclodextrin (RAMEB) and heptakis(2,3,6-tri-O-methyl)- β -cyclodextrin, were obtained and investigated both in solution and in solid state. The kneading method was used to prepare the inclusion complexes, and they were characterized with different analytical techniques, including thermal analysis, powder X-ray diffractometry, universal attenuated total reflectance Fourier-transform IR spectroscopy and UV spectroscopy. The stoichiometry of both APR/CDs inclusion complexes was found as 1:2 by employing continuous variation method. Benesi–Hildebrand equation was used for the apparent constant stability determination. Structural studies of the inclusion complexes were carried out using molecular modeling techniques in order to explain the complexation mechanism. The results of the studies demonstrate that the physicochemical properties of the kneaded products are different from ARP, testifying the inclusion complexes formation between aripiprazole and CDs when the kneading method is used. The solubility of the drug substance was improved upon complexation with CDs; higher increase in ARP solubility was noticed in the presence of RAMEB.

Keywords Aripiprazole · Cyclodextrins · Inclusion complexes · Thermal analysis · Solubility

Introduction

Aripiprazole (ARP), 7-[4-[4-(2,3-dichlorophenyl)piperazin-1-yl]butoxy]-3,4-dihydro-1H-quinolin-2-one (Fig. 1) is an atypical antipsychotic drug with a unique mechanism of

action used for the treatment of schizophrenia and mania in type I bipolar disorder [1, 2]. ARP is a quinolinone derivative, having poor aqueous solubility ($10.98 \pm 1.39 \text{ ng mL}^{-1}$) and high lipophilicity (Log *P* of 4.55), which makes it a Class II candidate of the Biopharmaceutics Classification

✉ Laura Sbârcea
sbarcea.laura@umft.ro

- ¹ Faculty of Industrial Chemistry and Environmental Engineering, Politehnica University of Timișoara, 2 Victoriei Square, 300006 Timișoara, Romania
- ² Department of Drug Analysis, Faculty of Pharmacy, “Victor Babeș” University of Medicine and Pharmacy, 2 Eftimie Murgu Square, 300041 Timișoara, Romania
- ³ Department of Analytical Chemistry, Faculty of Pharmacy, “Victor Babeș” University of Medicine and Pharmacy, 2 Eftimie Murgu Square, 300041 Timișoara, Romania
- ⁴ Research Center for Thermal Analysis in Environmental Problems, Faculty of Chemistry-Biology-Geography, West University of Timișoara, 16 Pestalozzi Street, Timișoara, Romania

⁵ Faculty of Physics, West University of Timișoara, 4 Vasile Pârvan Blvd, 300223 Timișoara, Romania

⁶ Department of Physical Chemistry, Faculty of Pharmacy, University of Medicine and Pharmacy Craiova, 2-4 Petru Rares Str., 200349 Craiova, Romania

⁷ Department of Dermatopharmacy and Cosmetology, Faculty of Pharmacy, “Victor Babeș” University of Medicine and Pharmacy, 2 Eftimie Murgu Square, 300041 Timișoara, Romania

⁸ Department of Physical Chemistry, Faculty of Pharmacy, “Victor Babeș” University of Medicine and Pharmacy, 2 Eftimie Murgu Square, 300041 Timișoara, Romania

System (BCS) [2, 3]. After oral administration, ARP undergoes high first-pass effect that leads to low therapeutic availability [4]. Aripiprazole possesses the ability to form a lot of polymorphs [5], which can exhibit different solubility, dissolution rates and stability, leading to the existence of non-equivalent bioavailabilities for different forms [6, 7].

Solubility is an essential property of drugs, being one of the most critical and important parameters influencing their bioavailability. Among the various approaches used to enhance the solubility of BCS II class drugs, inclusion of the active pharmaceutical ingredients in cyclodextrin is a valuable one [7].

Cyclodextrins (CDs) are cyclic glucose oligomers built up from glucopyranose units linked by 1,4- α -glycosidic bonds. The three major types of CDs consist of six, seven or eight glucose units (α , β and γ -cyclodextrin, respectively). CDs molecules have a hydrophilic outer surface, making them water-soluble and a hydrophobic internal cavity available to form non-covalent host-guest inclusion complexes with numerous drug molecules of appropriate shape and size [8–12]. The encapsulation of the drug in the cyclodextrin cavity has gained pharmaceutical interest as physicochemical and biopharmaceutical properties of the guest, such as aqueous solubility, physical and chemical stability, melting point, volatility, unpleasant taste or odors, drug delivery through biological membranes, are notably changed by its inclusion [11–20]. Furthermore, CDs are used to alleviate the gastrointestinal irritation and prevent the incompatibilities between drug substances and excipients [8, 15, 21]. Therefore, the CD complexation leads to considerable improvement in drugs pharmaceutical formulations and enhancement of solubility, dissolution, bioavailability and biological activity of drugs [11, 12, 15, 22–24]. Among the CDs, β -cyclodextrin (β -CD) has achieved pharmaceutical relevance despite its low aqueous solubility. The random substitution of any β -cyclodextrin hydroxyl group creates a disruption of stable hydrogen bond system around the cyclodextrin rims producing an intensive enhancement of its aqueous solubility. Thus, several CD derivatives of pharmaceutical interest have been developed, among them methylated β -CDs [25].

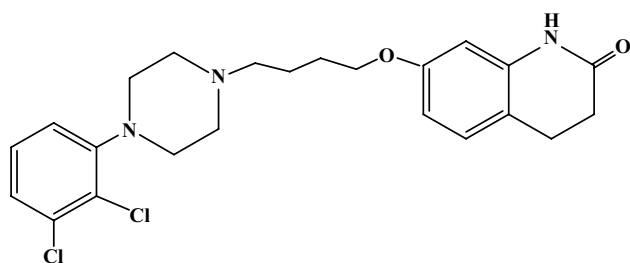


Fig. 1 Chemical structure of aripiprazole (ARP)

There are few studies regarding the use of CDs in increasing ARP water solubility. Mihajlovic et al. [26] studied the inclusion of ARP in hydroxypropyl- β -CD (HP- β -CD) cavity. They observed higher solubility and dissolution rate for the ARP/HP- β -CD spray-dried inclusion complexes. Badr-Eldin SM et al. [27] formulated the inclusion complexes of ARP with β -CD and HP- β -CD using kneading, microwave irradiation and freeze-drying techniques in a molar ratio of 1:1 and 1:2 (drug to CD). They reported an important solubility and dissolution enhancement in the case of 1:2 molar ratio ARP/HP- β -CD freeze-dried product. In addition, there is already a product containing the inclusion complex of ARP with sulfobutylether- β -CD marketed by Otsuka Pharmaceutical Company (Tokyo, Japan) under the brand name Abilify[®] as an intramuscular injectable solution [26].

The role of random methyl- β -cyclodextrin (RAMEB) and heptakis(2,3,6-tri-O-methyl)- β -cyclodextrin (TRIMEB) in improving oral drug dissolution rate is based on the important rise in the aqueous solubility of the two CDs and the affinity for the hydrophobic molecules compared to the parent compound [28, 29].

In order to increase ARP solubility, this paper aimed to obtain and completely characterize the inclusion complexes of ARP with two β -CD derivatives, namely RAMEB and TRIMEB. The binary products obtained by employing the kneading method and their correspondent physical mixtures have been characterized using UV spectroscopy, thermal analyses, PXRD and FTIR spectroscopy, both in solid state and in solution. The saturation solubility studies were further conducted in order to investigate the physicochemical performance of prepared kneaded products (KP).

Experimental

Materials

Aripiprazole (Pharmaceutical Secondary Standard) was purchased from Sigma-Aldrich. The two cyclodextrins, random methyl- β -cyclodextrin (DS~12) and heptakis(2,3,6-tri-O-methyl)- β -cyclodextrin were purchased from Cyclolab R&L Ltd (Budapest, Hungary). All substances were used as received. All other chemicals and reagents used in this study were of analytical grade.

Characterization of inclusion complexes in solution

All UV spectra were carried out using SPECTRONIC UNICAM—UV 300 UV-visible double-beam spectrophotometer with 1-cm matched quartz cells.

The stoichiometry of the host-guest inclusion complexes was determined by employing Job's method [14, 30]. UV

spectroscopic measurements were used in order to generate the Job's plot. For this purpose, equimolar 9.00×10^{-5} M solutions of ARP and CDs (RAMEB and TRIMEB, respectively) prepared in 0.1M acetate buffer (pH 4.0) were mixed to a standard volume, varying the molar ratio of the guest from 0.0 to 1.0, keeping the total concentration of the substances constant. A similar dilution set of the ARP stock solution was also obtained employing the same solvent. After stirring, the absorbance of all solution was recorded at 249 nm. The difference in absorbance, ΔA ($\Delta A = A - A_0$) of ARP in the presence (A) and in the absence (A_0) of CDs was plotted against ARP mole fraction R ; $R = [\text{ARP}] / \{[\text{ARP}] + [\text{CD}]\}$.

Benesi–Hildebrand method was performed for determining the apparent stability constants of the ARP/CDs inclusion complexes. The absorption measurements were recorded for ARP in the presence of increasing concentration of CDs and also under free complexation conditions. The ARP concentration was maintained constant, at 6.48×10^{-5} M in 0.1M acetate buffer (pH 4.0), and the CDs concentration was varied from 0 to 1.30×10^{-3} M, in the same solvent. Spectra were recorded in the range of 200–310 nm, using 1.0-cm quartz cells. All the experiments were carried out in triplicate.

The binding constants determination is achieved by using the changes in absorbance at wavelength of 249 nm for ARP in the presence of increasing CD concentration. The stability constants values can be calculated using the Benesi–Hildebrand equation for 1:2 stoichiometry of the guest–host inclusion complex [31, 32]:

$$\frac{1}{\Delta A} = \frac{1}{\Delta \varepsilon \cdot [\text{ARP}] \cdot K \cdot [\text{CD}]^2} + \frac{1}{\Delta \varepsilon \cdot [\text{ARP}]} \quad (1)$$

where $\Delta \varepsilon$ is change in molar attenuation coefficient, ΔA is change in absorbance and K , stability constant.

Preparation of the solid inclusion complexes and physical mixtures

The ARP/RAMEB and ARP/TRIMEB inclusion complexes were prepared employing the kneading method and 1:1 molar ratio. This method was chosen because of its simplicity, rapidity, accessibility and economic advantages when compared to other methods [33]. For the ARP/RAMEB inclusion complex preparation, the amounts of 0.0508 g ARP and 0.1499 g RAMEB were weighed and the obtained mixture was pulverized in a mortar and triturated with 0.20 g ethanol/HCl 0.1M solution (1:1, m/m). In the case of ARP/TRIMEB binary product, 0.0717 g ARP and 0.2287 g TRIMEB were accurately weighed and the obtained mixture was pulverized and triturated with 0.30 g ethanol/HCl 0.1M solution (1:1, m/m) in order to obtain a homogeneous paste. The

paste was kneaded for 45 min, and an appropriate quantity of solvent was added during this process in order to maintain a suitable consistency. The product thus obtained was dried at ambient temperature and then in the oven, at 40 °C for 24 h. The dried kneaded products were pulverized and passed through a 75- μm -size sieve.

Additionally, physical mixtures consisting of ARP and every cyclodextrin in the same molar ratio as the inclusion complexes were prepared. Aripiprazole and the host substances were mixed together in the mortar and pestle for 10 min, in the absence of the solvent.

Characterization of solid-state binary systems

Thermal analysis

TG/DTG/HF measurements were acquired using a PerkinElmer DIAMOND TG/DTA instrument. The thermal behavior of ARP, CDs, physical mixtures and kneaded products was evaluated by using samples of about 3–4 mg in aluminum crucibles, under air atmosphere at a flow rate of 100 mL min^{-1} , over the temperature range of 40–500 °C, with heating rate of 10 °C min^{-1} .

Powder X-ray diffractometry

Data collection was carried out using a Bruker D8 Advance powder X-ray diffractometer. The X-ray diffraction patterns were collected at ambient temperature, using $\text{CuK}\alpha$ radiation (40 kV, 40 mA) and a Ni filter, over the interval of 10–45° angular domain (2θ).

Fourier-transform infrared spectroscopy

The FTIR spectra of ARP, RAMEB, TIMEB, ARP/CDs kneaded products and physical mixtures were obtained using a PerkinElmer SPECTRUM 100 device. The analysis was carried out directly on solid samples, in the 4000–600 cm^{-1} spectral domain on an UATR device. Spectra were built up after 16 co-added acquisitions, with a spectral resolution of 4 cm^{-1} .

Molecular modeling

Three-dimensional coordinates of ARP were generated using the Gaussian program suite at DFT/B3LYP/6-311G optimization. To gain insight into the interaction between ARP and the two CDs, RAMEB and TRIMEB, the molecular docking technique was used. The RAMEB structure used in this work was generated from the curated coordinates of ligand 2QKH (X-ray diffraction, resolution 1.9 Å) downloaded

from the Protein Data Bank database [34]. Methyl groups were manually added on free hydroxyl groups in order to obtain a degree of substitution equal with 12 (GaussView 5, Semichem Inc). Substituents were added on the β -CD natural core, namely 4 $-\text{CH}_3$ on the O2- position for the 2, 3, 4 and 6 glucopyranose units, 5 groups on the O3- for the 1, 2, 4, 5, 7 glucose residues and finally 3 $-\text{CH}_3$ on 1, 5, 7 glucopyranose units O6- position. For TRIMEB, the same initial β -CD was used, methyl groups being manually added on all free hydroxyl groups in order to obtain a fully permethylated structure (GaussView 5, Semichem Inc). Both RAMEB and TRIMEB were optimized in the same manner with ARP (DFT/B3LYP/6-311G). All dihedral angles of the methoxy groups were homogenized, the resulting conformations being compatible with an unhindered CD cavity.

As a single molecule of ARP was expected to accommodate with 2 molecules of CDs, two consecutive docking cycles were carried out starting and selecting the best result from each cycle. CDs dimers were generated from two identical CD molecules aligned on the cavity axes, with the outer sides pointing one to another. In the first docking, two molecules of CD were used, one as a receptor and the other like a ligand in order to obtain the best configuration of the dimer complex and to compute the total interaction energy (kcal mol^{-1}). In the second docking, ARP as a ligand and CDs dimers as receptors were used.

The molecular docking analysis was carried out in vacuum using the AutoDock 4.2.6 software and the AutoDockTools. The preparation of CDs dimers molecule and the docking between ARP and dimers involve adding all the polar hydrogens, computing the Gasteiger charge; grid box was created using Autogrid 4 with $50 \times 50 \times 50 \text{ \AA}$ in x , y and z directions with 0.375 \AA spacing from CD center. The Lamarckian genetic algorithm with a population size of 150 and a number of 50 runs was applied in the docking process. All the other parameters were used with the default values. Molecular modeling figures were generated using PyMol [35].

Solubility profile of kneaded products

In order to evaluate the change in solubility due to the complexation, the saturation shake-flask method was employed. An excess amount of ARP, ARP/RAMEB and ARP/TRIMEB binary systems was added in 5 mL of acetate buffer 0.1M (pH 4.0) so that saturated solutions were obtained. The samples were shaken 24 h at the ambient temperature and then, the insoluble drug substance was removed by filtration using $0.45\text{-}\mu\text{m}$ cellulose acetate filter. After appropriate dilution, the absorption intensity of the filtrate was recorded at 249 nm. The drug substance content was evaluated by means of ARP calibration curve. To obtain the standard curve, a set of ARP solution in acetate buffer 0.1M (pH 4.0) with

concentration ranging between 2.64 and $40.36 \mu\text{g mL}^{-1}$ was prepared. The absorbance of the calibration standards was recorded at 249 nm, and the data were used in order to obtain a standard curve plotting the concentration (C , $\mu\text{g mL}^{-1}$) on the x -axis and absorbance (A) on the y -axis. The ARP calibration curve is described by the equation: $A = 0.02848 \cdot C - 0.0078$, with $R = 1$.

Results and discussion

Characterization of inclusion complexes in solution

Stoichiometry and stability constant determination

According to Job's method [36], the stoichiometry of the inclusion complex is given by the value of the molar ratio R which indicates the maximum concentration of the complex, when a measurable parameter that correlates linearly with the complex concentration (i.e., absorbance) is plotted against guest mole fraction. The maximum point of molar ratio corresponds to the complexation stoichiometry [14, 15, 30].

The maximum absorbance variation (ΔA) for ARP in the presence of both RAMEB and TRIMEB (Fig. 2) is reached when ARP mole fraction is 0.33, thus indicating that both inclusion complexes were formed with 1:2 guest/host stoichiometry.

The Benesi–Hildebrand method is the classical approach to estimate the stoichiometry and binding constant of the inclusion complexes [14, 30, 31, 37]. In order to confirm the stoichiometry and to obtain the binding constants of the inclusion complexes, changes in the UV absorption intensity signals of ARP at 249 nm in the absence and in the presence of CDs have been measured. An increase in ARP absorption intensity as a consequence of increasing concentrations of both CDs has been noticed (Fig. 3a, c), along with a bathochromic shift in the absorption maxima of ARP in the presence of RAMEB (Fig. 3c), demonstrating the inclusion complexes formation.

In order to confirm the 1:2 stoichiometry for ARP and the two cyclodextrins inclusion complexes, double reciprocal plots were represented ΔA^{-1} versus $[\text{CD}]^{-2}$, as they are presented in Fig. 3b, d. For each of CDs, the plot ΔA^{-1} versus $[\text{CD}]^{-2}$ was linear, with correlation coefficient values $R^2 = 0.9889$ for RAMEB and $R^2 = 0.9877$ in the case of TRIMEB, thus proving the formation of 1:2 ARP/CD inclusion complexes.

The values of the binding constants were evaluated using Benesi–Hildebrand Eq. (1) as a ratio of the intercept to slope of the straight line in the Benesi–Hildebrand double reciprocal plot. The stability constants values were determined as $(6.09 \pm 0.05) \times 10^6 \text{ M}^{-2}$ for ARP/RAMEB inclusion complex

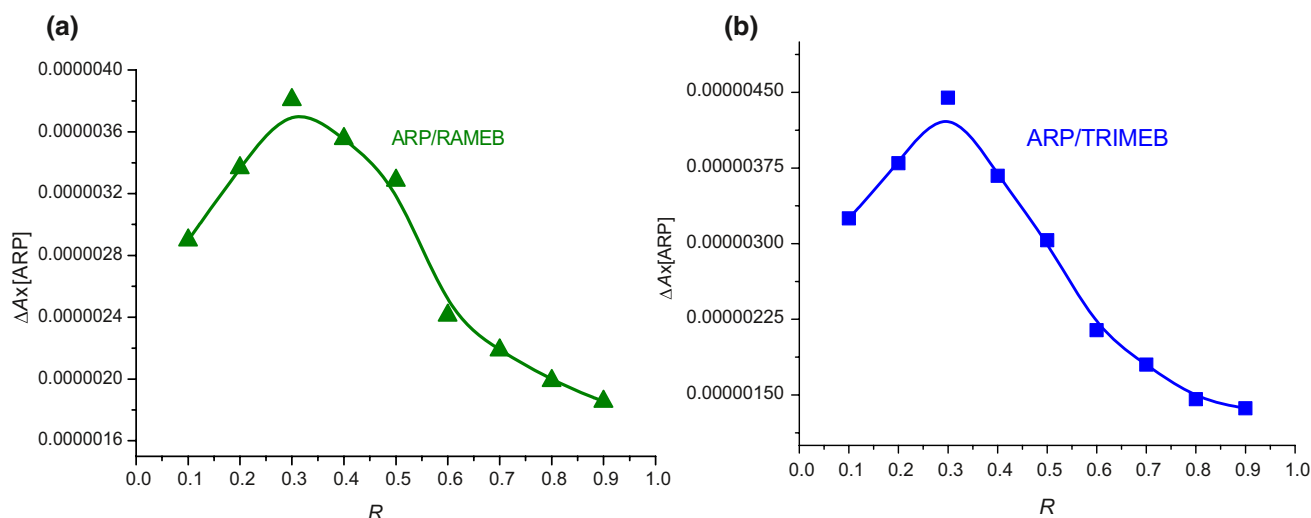


Fig. 2 Job's plot for ARP/RAMEB (a) and ARP/TRIMEB (b) inclusion complexes at 249 nm in acetate buffer 0.1M (pH 4.0)

and $(6.12 \pm 0.09) \times 10^6 \text{ M}^{-2}$ in the case of ARP/TRIMEB binary system.

Characterization of solid-state inclusion complexes

Thermal analysis

The thermoanalytical curves (TG/DTG/HF) of ARP, RAMEB, TRIMEB, ARP/RAMEB and ARP/TRIMEB prepared by physical mixture (PM) and kneading method are shown in Fig. 4a–g.

The TG/DTG curves of ARP indicate a very small mass loss that begins at 148.3 °C, with a $\text{DTG}_{\text{max}} = 148.7 \text{ °C}$ ($\Delta m = 0.4\%$). The ARP decomposition takes place in one step [38], starting around 220 °C, $\text{DTG}_{\text{max}} = 301.7 \text{ °C}$, as shown in Fig. 4a, indicating a good thermal stability of the drug substance. The HF curve of ARP reveals two endothermic events, one at 139.1 °C, corresponding to the melting of polymorphic form III and another at 148.7 °C, attributed to the melting of form I, these indicating the polymorphic transition from metastable form III to form I with the highest thermodynamic stability [39]. An exothermic effect ($T_{\text{peak}} = 316.2 \text{ °C}$) is also noticed in the HF curve of ARP corresponding to its thermal degradation.

The thermal curves of RAMEB indicate a small mass loss between 40 °C and 85 °C ($\Delta m = 5.3\%$) accompanied by endothermic effect ($T_{\text{peak}} = 52.0 \text{ °C}$) that corresponds to the CD crystallization water loss (Fig. 4b). The RAMEB dehydration is followed by a stability stage between 85 and 270 °C, but after 270 °C the mass loss continues and the degradation process occurs as the exothermic peak effect ($T_{\text{peak}} = 361.0 \text{ °C}$) of the HF curve indicates.

The thermoanalytical curves of ARP/RAMEB binary systems reveal differences in comparison with those of the pure substances. The disappearance of the endothermic melting peak of ARP form III can be noticed in the HF curves of both ARP/RAMEB PM and KP and the displacement at higher temperature of the endothermic melting event of ARP form I, which appears at 157.7 °C in the HF curve of PM (Fig. 4c) and at 169.1 °C in the KP thermal curve (Fig. 4d). Furthermore, the RAMEB decomposition exothermic peak is shifted toward lower temperature in the HF diagram of KP ($T_{\text{peak}} = 334.9 \text{ °C}$) and to higher temperature in the case of PM curve ($T_{\text{peak}} = 365.1 \text{ °C}$).

The HF curve of TRIMEB exhibits an endothermic event with a maximum at 161 °C due to the melting of CD (Fig. 4e). A good thermal stability is noticed for TRIMEB up to 190 °C as the TG profile shows, the main decomposition process starting at 190, with a $\text{DTG}_{\text{max}} = 348.0 \text{ °C}$. According to the HF curve, this process is accompanied by an exothermic event with a maximum at 348.0 °C.

Differences are also noticed in the case of thermal behavior of the binary systems ARP/TRIMEB PM and KP in relation to that of the parent compounds. Thus, the disappearance of the endothermic melting peak of ARP form III is observed in the HF curve of ARP/TRIMEB KP. The two melting endothermic peaks of ARP are shifted toward lower temperature 128.8 °C and 146.1 °C, respectively, in the HF diagram of ARP/TRIMEB PM. Also, the exothermic event corresponding to the TRIMEB decomposition is displaced to higher temperature in the HF curve of both PM ($T_{\text{peak}} = 369.4 \text{ °C}$) and KP ($T_{\text{peak}} = 360.8 \text{ °C}$).

The thermal analysis leads to valuable outcome regarding the interaction between host and guest molecules during the inclusion complex formation. When the guest molecules

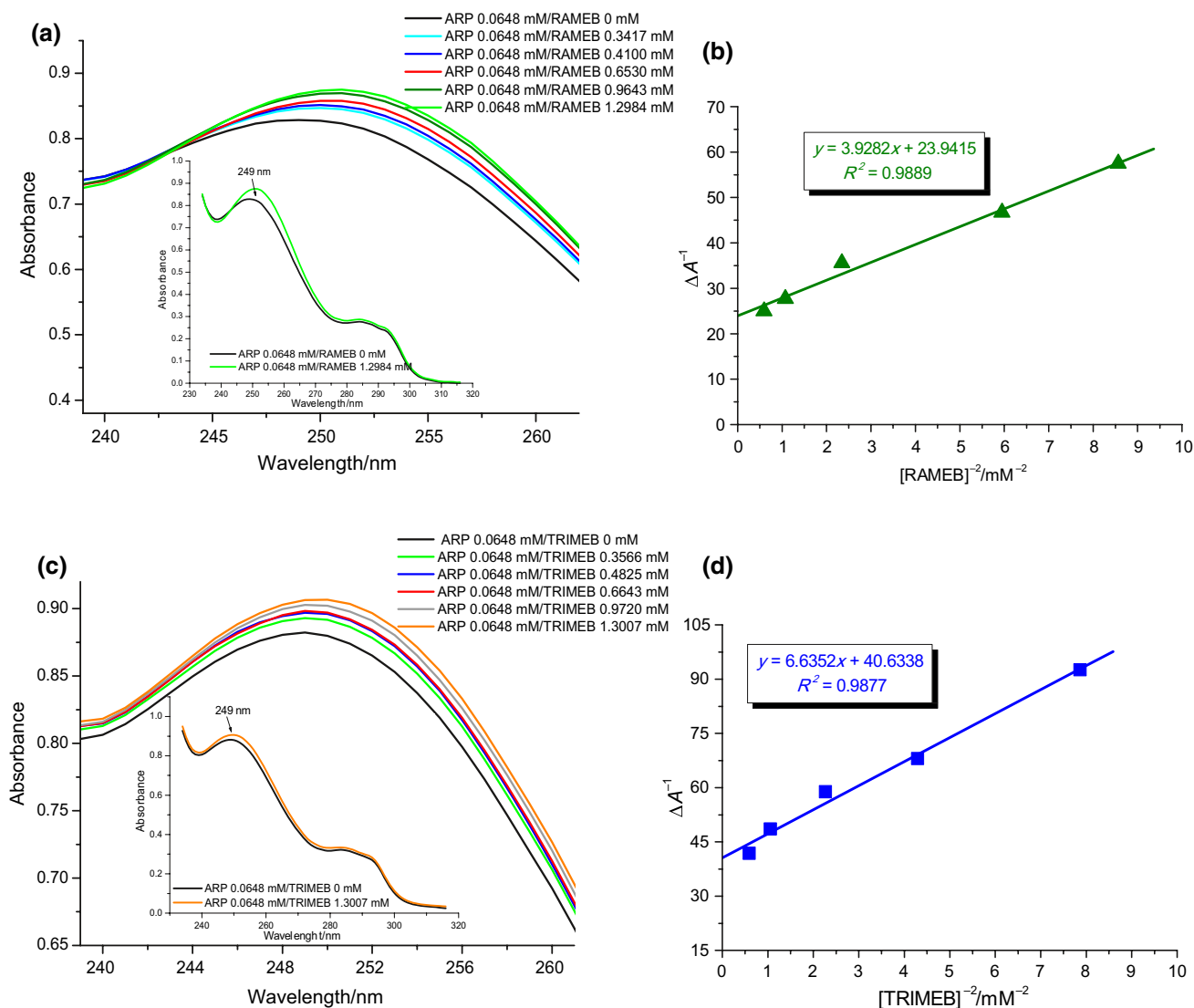


Fig. 3 UV spectra of pure ARP and ARP/CD inclusion complex, in acetate buffer (pH 4.0), in the presence of increasing CD concentration, 239–262 nm spectral domain—main image; UV spectra of pure ARP and ARP/CD at maximum CD concentration, in spectral range

of 235–310 nm—inserted image: ARP/RAMEB (a) and ARP/TRIMEB inclusion complex (c); Benesi-Hildebrand linear plots for $1/\Delta A$ versus $1/[RAMEB]^2$ (b) and for $1/\Delta A$ versus $1/[TRIMEB]^2$ (d)

are entrapped in the CDs cavity, their melting point generally shifts to a different temperature or disappears [40]. The absence of melting process of ARP form III from the thermal profile of the kneaded products ARP/RAMEB and ARP/TRIMEB along with the shift toward higher temperature of the melting of ARP form I indicates ARP involvement in the complexation process. The results obtained by using the thermal analysis strongly suggest the existence of an interaction between the drug substance and the two CDs and the formation of inclusion complexes in solid state.

Powder X-ray diffractometry

The PXRD patterns of ARP, RAMEB, TRIMEB and their corresponding PM and KP are presented in Fig. 5.

The ARP diffractometric profile reveals the presence of two peaks of higher intensity at 2θ value of 20.38 and 22.04 beyond several secondary peaks at 11.02; 14.36; 16.54 and 19.39 2θ , confirming the ARP polymorphic form III [39] and indicating its crystalline nature. The diffraction pattern of RAMEB has two broad peaks and many undefined, diffused peaks with low intensities, reflecting the amorphous nature of cyclodextrin [16]. The diffractograms of the binary compounds, both KP and PM present considerable reduction in the intensity of ARP major peaks and many undefined and

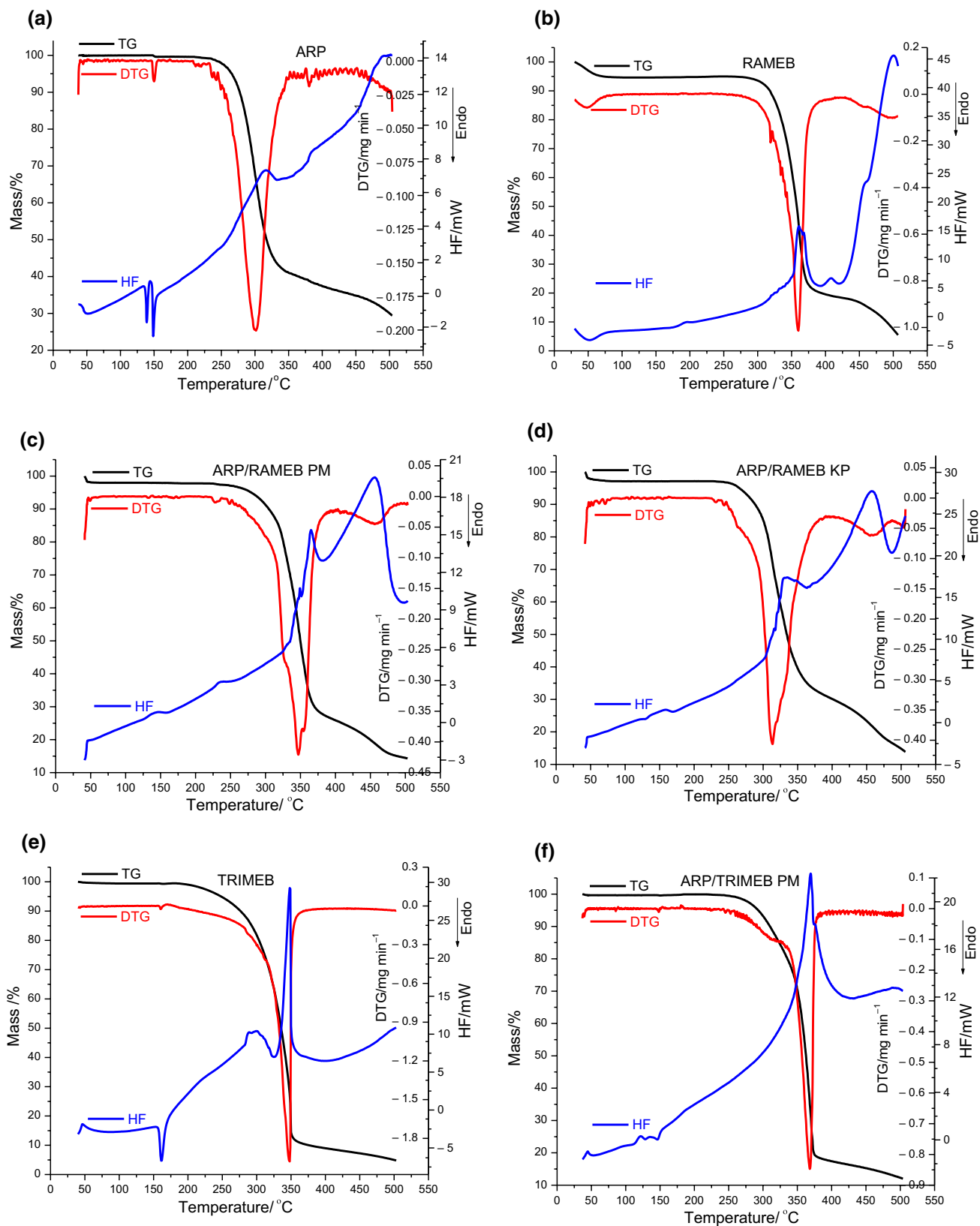


Fig. 4 TG, DTG and HF thermal curves of: ARP (a), RAMEB (b), ARP/RAMEB PM (c), ARP/RAMEB KP (d), TRIMEB (e), ARP/TRIMEB PM (f) and ARP/TRIMEB KP (g) in air atmosphere (100 mL min⁻¹), temperature range of 40–500 °C and heating rate of 10 °C min⁻¹

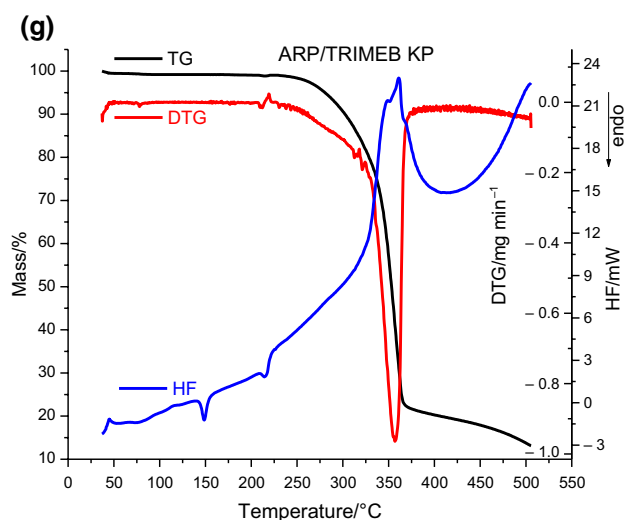


Fig. 4 (continued)

diffused peaks, similar to that of pure RAMEB, indicating the amorphous state of the compounds.

The crystalline nature of TRIMEB is clearly demonstrated by the appearance of sharp peaks at 8.14; 9.73; 10.84; 12.58; 15.31; 17.09; 19.40; 22.57 2θ in its diffractogram [41]. The PXRD pattern of ARP/TRIMEB PM presents a diminution of the characteristic diffraction peaks of drug substance and CD, indicating that the new compound is less crystalline than the ARP and the TRIMEB alone. The ARP/TRIMEB KP diffractometric profile has two broad peaks, fewer, less intense CD peaks and the absence of the ARP sharp characteristic peaks, thus suggesting that ARP is in an amorphous state.

Therefore, the reduction in crystallinity attributed to the ARP/RAMEB and ARP/TRIMEB KP suggests that ARP form with CDs inclusion complexes in solid state, demonstrating that new compounds are formed.

UATR-FTIR analysis

Figure 6 illustrates the UATR-FTIR spectra of pure ARP, RAMEB, TRIMEB, the ARP/CDs kneaded products and their corresponding physical mixtures. The IR spectra of the KP have been evaluated as compared to those of the parent substances in order to assess the inclusion complexes formation.

The UATR-FTIR spectrum of ARP presents characteristic bands of polymorph III [39, 42]. Specifically, the C=O stretching vibration from lactam ring appears as a strong band at 1676 cm^{-1} , the N–H stretching vibration band is located at 3192 cm^{-1} while the N–H bending vibration is identified at 1627 cm^{-1} [27]. ARP spectral pattern also presents other characteristic bands for ether group ($\text{C}_{\text{ar}}\text{-O}$ stretching vibration at 1259 cm^{-1}) and for aromatic ring (C=C–C stretching vibration at 1594 and 1576 cm^{-1} ; $\text{C}_{\text{ar}}\text{-H}$ wagging vibration at 806 and 778 cm^{-1} ; ortho Cl– C_{ar} stretch vibration at 1030 and 1047 cm^{-1} ; $\text{C}_{\text{ar}}\text{-CH}$ from dihydroquinoline-2-one ring wagging vibration at 1522 cm^{-1}) [43, 44]. C–H stretching vibration CH_2 arises at 2945 and 2812 cm^{-1} , and bending vibration appears at 1444 and 1375 cm^{-1} [26, 44].

RAMEB exhibits a broad absorption band in the $3600\text{--}3100\text{ cm}^{-1}$ region assigned to O–H stretching vibration from the non-methylated hydroxyl moieties and a large

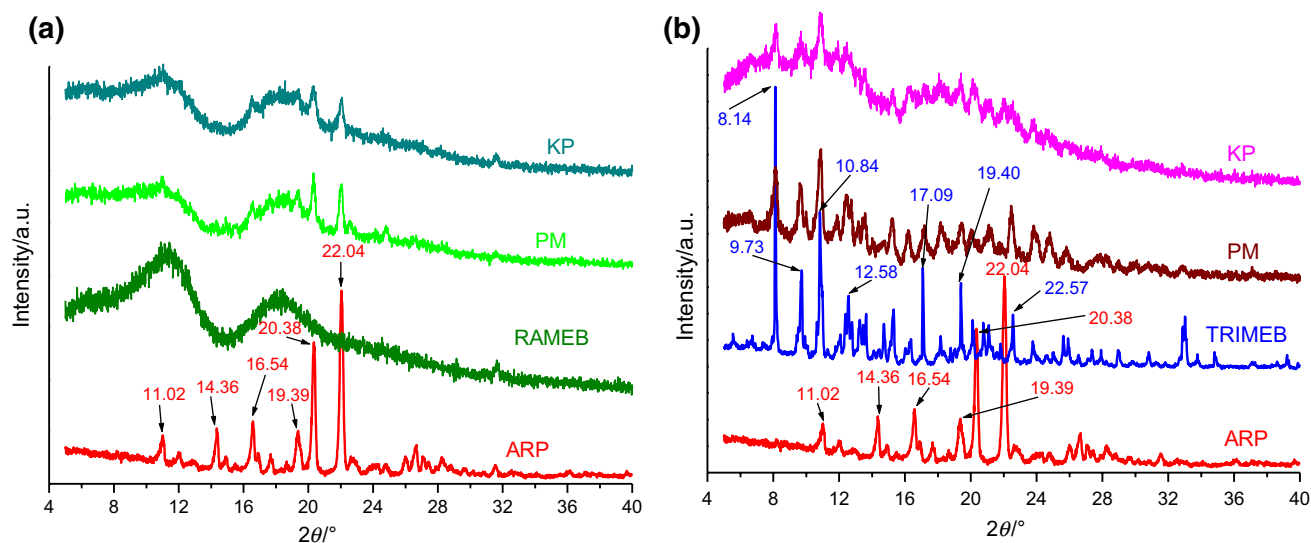


Fig. 5 X-ray diffraction pattern ARP, RAMEB, ARP/RAMEB PM and KP (a); ARP, TRIMEB and their PM and KP (b)

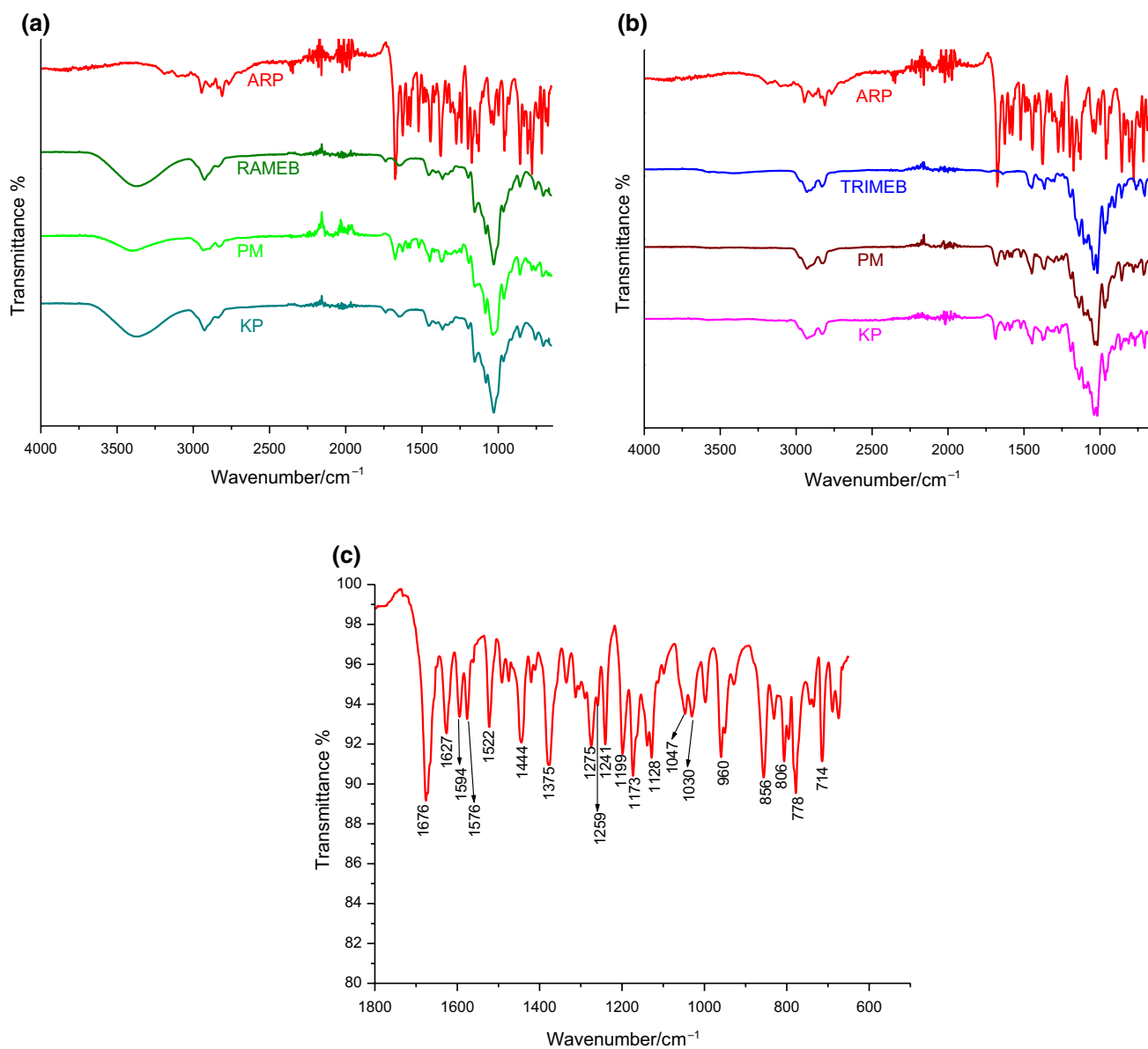


Fig. 6 UATR-FTIR spectra of ARP, RAMEB and their PM and KP (a); ARP, TRIMEB and their corresponding PM and KP (b) ARP in spectral range of 1800–600 cm^{-1} (c)

region below 1500 cm^{-1} which displays distinct peaks, most probably characteristic to the cyclodextrin ring [17, 45].

The IR spectra of both ARP/RAMEB KP and PM reveal considerable differences in comparison with the pure compounds. As Fig. 6 shows, the ARP characteristic peaks either have reduced their intensity along with shifting to different wavenumbers or have disappeared in the binary products. By analysis of the spectral data, we found that the ARP characteristic bands corresponding to the C=O stretching vibration and the skeletal vibration of the aromatic ring shifted from 1676 to 1576 cm^{-1} in the pure compound to 1677 and 1578 cm^{-1} in the PM and they are no more present in the KP spectrum. Also, the ARP characteristic bands from 1627,

1444 and 1376 cm^{-1} shifted to different wavenumbers in the ARP/RAMEB KP spectrum, namely 1639, 1452 and 1365 cm^{-1} , respectively. The intensity of ARP spectral bands in the KP is rather low in relation with the PM spectrum, where the drug presents higher intensity bands, thus highlighting weaker interaction between ARP and RAMEB when physically mixed (Fig. 6a).

In the UATR-FTIR spectrum of TRIMEB, the characteristic peaks have been identified at 2929 cm^{-1} assigned to symmetric and asymmetric C–H stretching vibration from CH_2 , at 1365 cm^{-1} due to C–H bending from CH_2 , at 1016 cm^{-1} associated to C–C–O stretching vibration and in the spectral region 1076–1022 cm^{-1} attributed to

C–O–C stretching vibrations, these being in agreement with previously reported data [41]. The broad band located in 3600–3100 cm^{-1} region (O–H stretching vibration), characteristic for RAMEB, was not observed in TRIMEB spectrum due to the methylation of the –OH moieties.

The IR spectroscopy results of the ARP/TRIMEB binary products prepared by physical mixture and kneading reveal changes in relation to the pure host and guest spectra. Thus, the ARP characteristic band corresponding to the C=O stretching vibration shifted to higher wavenumbers, 1677 and 1686 cm^{-1} , in the spectra of PM and KP, and the ARP band assigned to C=C–C stretching vibration shifted from 1576 cm^{-1} in pure drug to 1578 and 1580 cm^{-1} in the PM and KP spectra, as a result of the existence of an interaction between ARP and TRIMEB.

Also, the peak corresponding to N–H stretching vibration band, situated at 3192 cm^{-1} in pure ARP spectra, is no more present in the spectra of ARP/CDs PM and KP, most probably due to the formation of H-bonding between drug substance and CDs.

Molecular modeling

Automated docking is widely used for prediction of biomolecular complexes in structure/function analysis and in molecular design. Dozens of effective methods are available, incorporating different trade-offs in molecular representation, energy evaluation, and conformational sampling to provide predictions with a reasonable computational effort. AutoDock combines an empirical free energy force field with a Lamarckian Genetic Algorithm, providing fast prediction of bound conformations with predicted free energies of association [46].

The force field evaluates binding in two steps. The ligand and target start in an unbound conformation. In the first step, the intramolecular energetics is estimated for the transition from these unbound states to the conformation of the ligand and target in the bound state. The second step then evaluates the intermolecular energetics of combining the two components in their bound conformation. The force field includes six pair-wise evaluations (V) and an estimate of the conformational entropy lost upon binding ($\otimes S_{\text{conf}}$):

$$\begin{aligned} \otimes G = & (V_{\text{boundL-L}} - V_{\text{unboundL-L}}) \\ & + (V_{\text{boundP-P}} - V_{\text{unboundP-P}}) \\ & + (V_{\text{boundP-L}} - V_{\text{unboundP-L}} + \otimes S_{\text{conf}}) \end{aligned}$$

where L refers to the “ligand” and P refers to the “protein” in a ligand–protein docking calculation. Each of the pair-wise energetic terms includes evaluations for dispersion/repulsion, hydrogen bonding, electrostatics, and desolvation.

Molecular modeling was used for an in-depth characterization of the interaction between ARP and RAMEB/TRIMEB in ratio 1:2. As the optimal distance between two RAMEB and TRIMEB molecules is not known, targets were initially generated from two identical CDs. We obtained dimers with the outer sides pointing one to another, aligned on the cavity axes, with distances between cavity centers $\sim 10 \text{ \AA}$.

The binding free energy values are calculated as follows: $-5.29 \text{ kcal mol}^{-1}$ for the 2 RAMEB/ARP inclusion complex and $-5.24 \text{ kcal mol}^{-1}$ for 2 TRIMEB/ARP. According to our data, the ARP/RAMEB inclusion complex is more stable than the ARP/TRIMEB, because it has a lower value of binding free energy. Figures 7 and 8 present the theoretical ARP/RAMEB and ARP/TRIMEB inclusion complexes, as rendered in the PyMOL molecular visualization system, simulated in 1:2 molar ratio.

By the 3D images of the ARP/RAMEB 1:2 interaction, the presence of two hydrogen bonds is noticed between N–H hydrogen of the 2-piperidinone heterocycle and the hydroxyl (position 6) of a glucopyranose unit with a length of 2.3 Å , and with the hydroxyl from second position of a neighboring glucopyranose (1.8 Å). The carbonyl group of the heterocycle forms a hydrogen bond with the distance of 2.8 Å with hydrogen hydroxyl from position 6 of a carbohydrate moiety.

Analyzing the 3D images of the ARP/TRIMEB 1:2 interaction, it was observed that a hydrogen bond is formed between the N–H hydrogen of the 2-piperidinone heterocycle and the hydroxyl (position 6) of a glucopyranose unit with a length of 2.6 Å . An intermolecular N–O bond of 2 Å is formed between ARP piperazine nitrogen and the oxygen in the pyranose ring of a carbohydrate moiety. With the second TRIMEB molecule, a hydrogen bond is formed between the ARP N–H hydrogen of the 2-piperidinone heterocycle and the oxygen of a methoxy group from second position, with the length of 2 Å . From estimated binding free energies, we can conclude that the ARP/RAMEB 1:2 complex has greater stability, in comparison with ARP/TRIMEB 1:2. There is a predictable correlation between the type of intermolecular bonds and the stability of the complexes. ARP binds through three hydrogen bonds to the RAMEB dimer (1.8 Å , 2.3 Å , 2.8 Å), while to the TRIMEB dimer it binds through two hydrogen bonds (2 Å and 2.6 Å) and a N–O bond, which is inferior in strength as compared to hydrogen bonding.

Solubility profile of kneaded products

In order to measure the ARP solubility as it is in the ARP/RAMEB KP and ARP/TRIMEB KP, the shake-flask technique [47–49] was applied. The concentration of the drug substance in the saturated solution was determined

Fig. 7 Geometry of 1:2 ARP/RAMEB inclusion complex. Images **a**, **b** and **d** show the inclusion complex from the narrow rim of RAMEB's cavity. ARP guest molecules are represented in mesh/surface/sphere colored by element, while RAMEB is represented in red and blue. Image **c** shows polar contacts between ARP and RAMEB, ARP is colored in purple, RAMEBs are colored in blue and green. (Color figure online)

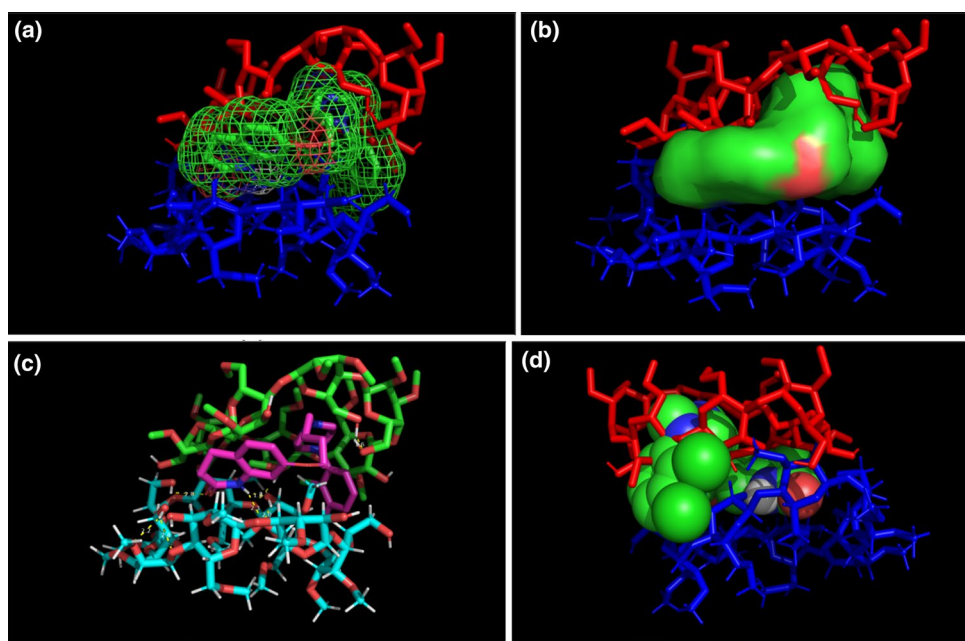
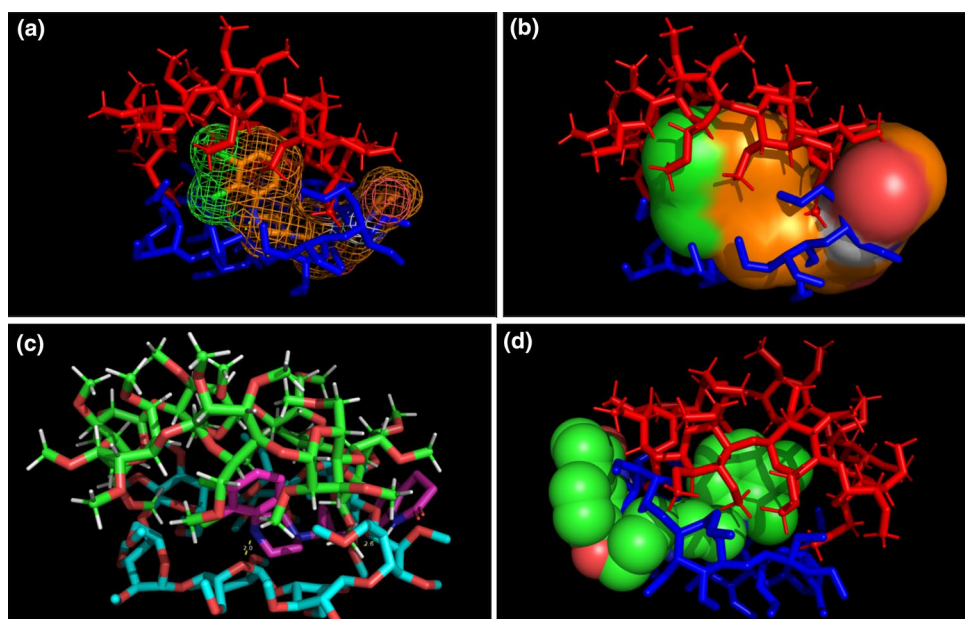


Fig. 8 ARP/TRIMEB inclusion complex simulation for 1:2 stoichiometry. Images **a**, **b** and **d** show the inclusion complex from the narrow rim of TRIMEB's cavity. ARP guest molecules are represented in mesh/surface/sphere colored by element and TRIMEB, in red and blue. Image **c** shows polar contacts between ARP and TRIMEB, ARP is colored in purple, TRIMEBs, in blue and green. (Color figure online)



spectrophotometrically, using a calibration curve of ARP, at 25 °C (Fig. 9).

The UV spectrophotometric measurements have indicated that the APR solubility in ARP/RAMEB KP and ARP/RAMEB KP is $671.35 \pm 0.01 \mu\text{g mL}^{-1}$ and $232.86 \pm 0.02 \mu\text{g mL}^{-1}$, respectively, as an average value of five experimental determinations. In standard controlled experiments, clear solutions were obtained by dissolving 13.20 mg of ARP/RAMEB KP and 4.90 mg of ARP/

TRIMEB KP in 5 mL 0.1M acetate buffer (pH 4), at ambient temperature.

The results of the saturation solubility studies highlighted that RAMEB and TRIMEB are efficient carriers for solubility enhancement of poorly soluble drug ARP. The ARP solubility in 0.1M acetate buffer (pH 4) is increased by 3.94-fold in the presence of TRIMEB and by 11.36-fold with RAMEB in comparison with free ARP ($59.09 \mu\text{g mL}^{-1}$) due to the solubilizing effect of CDs.

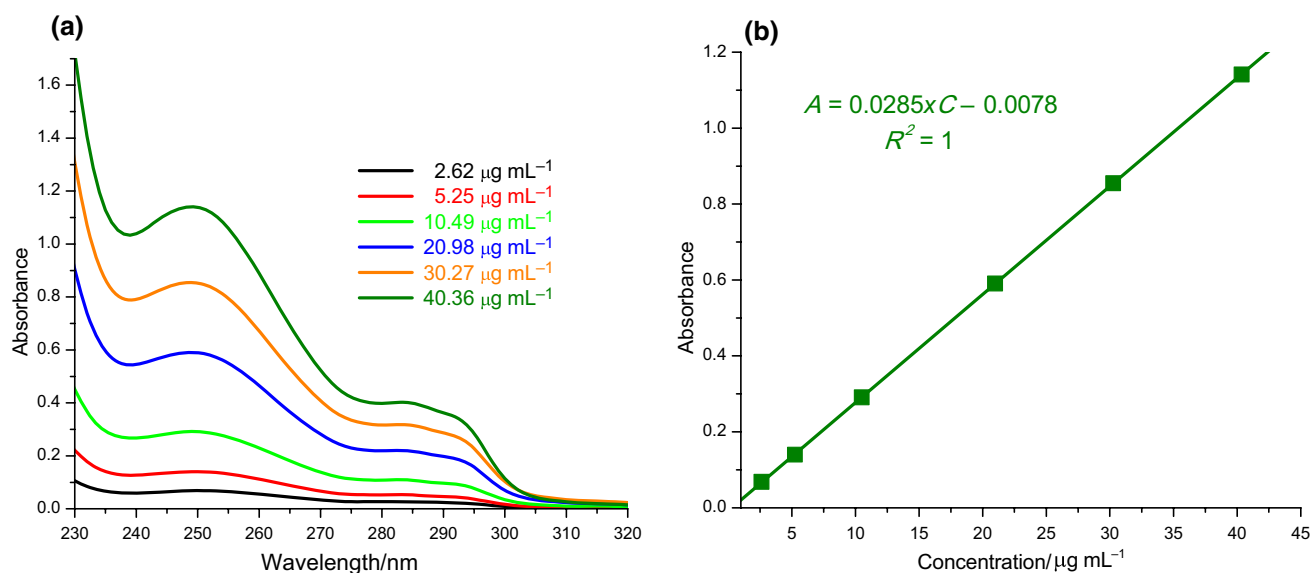


Fig. 9 Absorption spectra of ARP solution in 0.1M acetate buffer (pH 4), at 25 °C (a); calibration curve of ARP (b)

Conclusions

The present study investigates the inclusion complexation behavior and characterization of aripiprazole with two CD derivatives, RAMEB and TRIMEB by theoretical and experimental approaches. The experimental results clearly demonstrate that real inclusion complexes were formed between ARP and the two CDs, when the kneading method was employed, with a 1:2 stoichiometry, as the Job's method indicated. The physicochemical properties of the kneaded products ARI/RAMEB and ARI/TRIMEB are different in relation to the pure precursors, as the thermal analysis, PXRD and UATR-FTIR spectroscopy highlighted. A significant enhancement in ARP solubility is demonstrated by the shake-flask method when RAMEB is used as host molecule.

References

- Di Sciascio G, Riva MA. Aripiprazole: from pharmacological profile to clinical use. *Neuropsychiatr Dis Treat*. 2015;11:2635–47.
- Casey AB, Canal CE. Classics in chemical neuroscience: aripiprazole. *ACS Chem Neurosci*. 2017;8(6):1135–46.
- Abdelbary AA, Elshafeey AH, El-Nabarawi M, Ellassasy A, Li X, Jasti B. Comparative in vivo evaluation of aripiprazole coprecipitate, nanoparticles and marketed tablets in healthy human volunteers and in vitro-in vivo correlation. *Curr Trends Biotechnol Pharm*. 2011;5(4):1397–409.
- Silki, Sinha VR. Enhancement of in vivo efficacy and oral bioavailability of aripiprazole with solid lipid nanoparticles. *AAPS PharmSciTech*. 2018;19(3):1264–73.
- Brittain HG. Aripiprazole: polymorphs and solvatomorphs. In: Brittain HG, editor. *Profile of drug substances, excipients and related methodology*, vol. 37. Amsterdam: Elsevier; 2012. p. 1–29.
- Saifee M, Inamdar N, Dhamecha D, Rathi A. Drug polymorphism: a review. *Int J Health Res*. 2009;2(4):291–306.
- Censi R, Di Martino P. Polymorph impact on the bioavailability and stability of poorly soluble drugs. *Molecules*. 2015;20:18759–76.
- Loftsson T, Jarho P, Masson M, Jarvinen T. Cyclodextrins in drug delivery. *Expert Opin Drug Deliv*. 2005;2:335–51.
- D'Aria F, Serri C, Niccoli M, Mayol L, Quagliariello V, Iaffaioli RV, Biondi M, Giancola C. Host-guest inclusion complex of quercetin and hydroxypropyl- β -cyclodextrin. *J Therm Anal Calorim*. 2017;130:451–6.
- Usacheva T, Kabirov D, Beregova D, Gamov G, Sharnin V, Biondi M, Mayol L, D'Aria F, Giancola C. Thermodynamics of complex formation between hydroxypropyl- β -cyclodextrin and quercetin in water-ethanol solvents at $T = 298.15$ K. *J Therm Anal Calorim*. 2019;138(1):417–24.
- Pires FQ, Pinho LA, Freire DO, Silva ICR, Sa-Barreto LL, Cardozo-Filho L, Gratieri T, Gelfuzo GM, Cunha-Filho M. Thermal analysis used to guide the production of thymol and *Lippia organoides* essential oil inclusion complexes with cyclodextrin. *J Therm Anal Calorim*. 2019;137(2):543–53.
- Júnior FJLR, da Silva KMA, Brandão DO, Junior JVC, dos Santos JAB, de Andrade FHD, de Araujo Batista RS, Lins TB, de Sousa DP, Dantas Medeiros AC, Conceição MM, Macêdo RO, de Souza FS. Investigation of the thermal behavior of inclusion complexes with antifungal activity. *J Therm Anal Calorim*. 2018;133(1):641–8.
- Garcia A, Leonardi D, Salazar MO, Lamas MC. Modified β -cyclodextrin inclusion complex to improve the physicochemical properties of albendazole: complete in vitro evaluation and characterization. *PLoS One*. 2014;9(2):e88234. <https://doi.org/10.1371/journal.pone.0088234>.
- Sbârcea L, Ledeti A, Udrescu L, Văruț RM, Barvinschi P, Vlase G, Ledeti I. Betulonic acid-cyclodextrin inclusion complexes. *J Therm Anal Calorim*. 2019;138:2787–97.
- Sbârcea L, Udrescu L, Ledeti I, Szabadai Z, Fuliș A, Sbârcea C. β -cyclodextrin inclusion complexes of lisinopril and zofenopril. Physicochemical characterization and compatibility study

- of lisinopril- β -cyclodextrin with lactose. *J Therm Anal Calorim.* 2016;123:2377–90.
16. Sbârcea L, Udrescu L, Drăgan L, Trandafirescu C, Szabadai Z, Bojiță M. Fosinopril–cyclodextrin inclusion complexes: phase solubility and physicochemical analysis. *Pharmazie.* 2011;66:584–9.
 17. Cîrcioban D, Ledeti A, Vlase G, Coricovac D, Moaca A, Farcaș C, Vlase T, Ledeti I, Dehelean C. Guest–host interactions and complex formation for artemisinin with cyclodextrins: instrumental analysis and evaluation of biological activity. *J Therm Anal Calorim.* 2018;134:1375–84.
 18. Brusnikina M, Silyukov O, Chislov M, Volkova T, Proshin A, Mazur A, Tolstoy P, Terekhova I. Effect of cyclodextrin complexation on solubility of novel anti-Alzheimer 1,2,4-thiadiazole derivative. *J Therm Anal Calorim.* 2017;130:443–50.
 19. Sbârcea L, Udrescu L, Drăgan L, Trandafirescu C, Sasca V, Barvinschi P, Bojiță M. Characterization of fosinopril natrium-hydroxypropil- β -cyclodextrin inclusion complex. *Rev Chim Buchar.* 2011;62(3):349–51.
 20. Ikeda H, Fukushima Y, Matsubara T, Inenaga M, Kawahara M, Yukawa M, Fujisawa M, Yukawa E, Aki H. Improving water solubility of nateglinide by complexation of β -cyclodextrin. *J Therm Anal Calorim.* 2016;123:1847–50.
 21. Sbârcea L, Ledeti I, Drăgan L, Kurunzi L, Fuliș A, Udrescu L. Fosinopril sodium–Hydroxypropyl- β -cyclodextrin inclusion complex: thermal decomposition kinetics and compatibility studies. *J Therm Anal Calorim.* 2015;120:981–90.
 22. Stella VJ, He Q. Cyclodextrins. *Toxicol Pathol.* 2008;36:30–42.
 23. Laza-Knoerr AL, Gref R, Couvreur P. Cyclodextrin for drug delivery. *J Drug Target.* 2010;18:645–56.
 24. Brusnikina M, Silyukov O, Chislov M, Volkova T, Proshin A, Terekhova I. New water-soluble dosage forms of 1,2,4-thiadiazole derivative on the basis of inclusion complexes with cyclodextrins. *J Therm Anal Calorim.* 2017;127:1815–24.
 25. Szente L, Szejtli. Highly soluble cyclodextrin derivatives: chemistry, properties, and trends in development. *Adv Drug Deliv Rev.* 1999;36:17–28.
 26. Mihajlovic T, Kachrimanis K, Graovac A, Djuric Z, Ibric S. Improvement of aripiprazole solubility by complexation with 2-Hydroxypropyl- β -cyclodextrin using spray drying technique. *AAPS PharmSciTech.* 2012;3(2):623–31.
 27. Badr-Eldin SM, Ahmed TA, Ismail HR. Aripiprazole-cyclodextrin binary systems for dissolution enhancement: effect of preparation technique, cyclodextrin type and molar ratio. *Iran J Basic Med Sci.* 2013;16:1223–31.
 28. Brewster ME, Loftsson T. Cyclodextrins as pharmaceutical solubilizers. *Adv Drug Deliv Rev.* 2007;59:645–66.
 29. Garcia A, Leonardi D, Vasconi MD, Hinrichsen LI, Lamas MC. Characterization of albendazole-randomly methylated- β -cyclodextrin inclusion complex and in vivo evaluation of its antihelminthic activity in a murine model of trichinellosis. *PLoS ONE.* 2014;9(11):e113296. <https://doi.org/10.1371/journal.pone.0113296>.
 30. Chislov M, Silyukov O, Kumeev R, Proshin A, Perlovich G, Terekhova I. Complex formation of cyclodextrins with some pharmacologically active 1,2,4-thiadiazole derivatives. *J Therm Anal Calorim.* 2017;127:1797–805.
 31. Benesi HA, Hildebrand JH. A spectrophotometric investigation of the interaction of iodine with aromatic hydrocarbons. *J Am Chem Soc.* 1949;71(8):2703–7.
 32. Srinivasan K, Stalin T, Sivakumar K. Spectral and electrochemical study of host–guest inclusion complex between 2,4-dinitrophenol and -cyclodextrin. *Spectrochimica Acta Part A.* 2012;94:89–100.
 33. Salústio J, Feio G, Figueirinhas JL, Pinto JF, Cabral Marques HM. The influence of the preparation methods on the inclusion of model drugs in a β -cyclodextrin cavity. *Eur J Pharm Biopharm.* 2009;71:377–86.
 34. Protein Data Bank. <http://www.pdb.org/pdb/home/home.do>. Accessed 15 Sept 2019.
 35. DeLano, W. L. PyMOL. DeLano Scientific, San Carlos, CA, 700, 2002.
 36. Job P. Formation and stability of inorganic complexes in solution. *Ann Chim.* 1928;9:113–203.
 37. Chalumot G, Yao C, Pino V, Anderson JL. Determining the stoichiometry and binding constants of inclusion complexes formed between aromatic compounds and β -cyclodextrin by solid-phase microextraction coupled to high-performance liquid chromatography. *J Chromatogr A.* 2009;1216:5242–8.
 38. Fouteris E, Tarantili PA, Karavas E, Bikiaris D. Poly(vinyl pyrrolidone)–poloxamer-188 solid dispersions prepared by hot melt extrusion. *J Therm Anal Calorim.* 2013;113(3):1037–47.
 39. Łaszcz M, Witkowska A. Studies of phase transitions in the aripiprazole solid dosage form. *J Pharm Biomed Anal.* 2016;117:298–303.
 40. Doile MM, Fortunato KA, Schmücker IC, Schucko SK, Silva MAS, Rodrigues PO. Physicochemical properties and dissolution studies of dexamethasone acetate- β -cyclodextrin inclusion complexes produced by different methods. *AAPS Pharm Sci Tech.* 2008;9:314–32.
 41. Lavorgna M, Iacovino R, Russo C, Di Donato C, Piscitelli C, Isidori M. A new approach for improving the antibacterial and tumor cytotoxic activities of pipemidic acid by including it in trimethyl- β -CYCLODEXTRIN. *Int J Mol Sci.* 2019;20(2):416.
 42. Braun DE, Gelbrich T, Kahlenberg V, Tessadri R, Wieser J, Griesser UJ. Conformational polymorphism in aripiprazole: preparation, stability and structure of five modifications. *J Pharm Sci.* 2009;98:2010–26.
 43. Lin-Vien D, Colthup NB, Fateley WG, Grasselli JG. The handbook of infrared and raman characteristic frequencies of organic molecules. New York: Academic Press; 1991.
 44. Febry A, Lestari LEDM, Indrayanto G. Aripiprazole. Profile of drug substances, excipients and related methodology. 2013;38:35–85.
 45. Mennini N, Maestrelli F, Cirri M, Mura P. Analysis of physicochemical properties of ternary systems of oxaprozin with randomly methylated- β -cyclodextrin and L-arginine aimed to improve the drug solubility. *J Pharm Biomed Anal.* 2016;129:350–8.
 46. Morris GM, Goodsell DS, Halliday RS, Huey R, Hart WE, Belew RK, Olson AJ. Automated docking using a Lamarckian genetic algorithm and an empirical binding free energy function. *J Comp Chem.* 1998;19:1639–62.
 47. Baka E, Comer JEA, Takács-Novák K. Study of equilibrium solubility measurement by saturation shake-flask method using hydrochlorothiazide as model compound. *J Pharm Biomed.* 2008;46:335–41.
 48. Detrich Á, Dömötör KJ, Katona MT, Markovits I, Láng JV. Polymorphic forms of bisoprolol fumarate. *J Therm Anal Calorim.* 2019;135(6):3043–55.
 49. Udrescu L, Sbârcea L, Fuliș A, Ledeti I, Vlase G, Barvinschi P, Kurunzi L. Physicochemical analysis and molecular modeling of the fosinopril β -cyclodextrin inclusion complex. *J Spectrosc Spetrosc-Int J.* 2014;2014:748468.